

Self-interacting superfluid dark matter droplets

Vicente Delgado¹ and Antonio Muñoz Mateo¹

¹*Departamento de Física, Facultad de Ciencias, Universidad de La Laguna, E-38200 La Laguna, Tenerife, Spain*

Accepted XXX. Received YYY; in original form ZZZ

ABSTRACT

We assume dark matter to be a cosmological self-gravitating Bose–Einstein condensate of non-relativistic ultralight scalar particles with competing gravitational and repulsive contact interactions and investigate the observational implications of such model. The system is unstable to the formation of stationary self-bound structures that minimize the energy functional. These *cosmological superfluid droplets*, which are the smallest possible gravitationally bound dark matter structures, exhibit a universal mass profile and a corresponding universal rotation curve. Assuming a hierarchical structure formation scenario where granular dark matter haloes grow around these primordial stationary droplets, the model predicts cored haloes with rotation curves that obey a single universal equation in the inner region ($r \lesssim 1$ kpc). A simultaneous fit to a selection of galaxies from the SPARC database chosen with the sole criterion of being strongly dark matter dominated even within the innermost region, indicates that the observational data are consistent with the presence of a Bose–Einstein condensate of ultralight scalar particles of mass $m \simeq 2.2 \times 10^{-22}$ eV c^{-2} and repulsive self-interactions characterized by a scattering length $a_s \simeq 7.8 \times 10^{-77}$ m. Such small self-interactions have profound consequences on cosmological scales. They induce a natural minimum scale length for the size of dark matter structures that makes all cores similar in length (~ 1 kpc) and contributes to lower their central densities.

Key words: cosmology: theory – dark matter – galaxies: haloes

1 INTRODUCTION

Despite the great success of the Lambda Cold Dark Matter (Λ CDM) model in describing the large-scale structure of the Universe, on smaller scales ($\lesssim 10$ kpc) a number of predictions of this model seem to be in clear disagreement with observational evidence (Weinberg et al. 2015; Bullock & Boylan-Kolchin 2017). In particular, CDM N-body simulations yield an overabundance of unobserved small-scale structure (Kauffmann et al. 1993; Klypin et al. 1999; Moore et al. 1999) and predict dark matter haloes with dense cuspy density profiles at their centres (Navarro et al. 1997), while observations in dwarf galaxies favour shallow cored halo profiles (Flores & Primack 1994; Moore 1994; Boylan-Kolchin et al. 2011). Observations also indicate that these dark-matter dominated galaxies have a minimum characteristic scale length as well as remarkably similar central densities over a wide range of luminosities, with a mass content within the innermost 300 pc of $\sim 10^7 M_\odot$ (Gilmore et al. 2007; Strigari et al. 2008). These results and, in general, the observed properties of the mass profiles at the centres of the haloes are difficult to explain within the standard pressureless CDM model.

While the problems of the CDM model can be alleviated in part by introducing specific baryonic physics (Weinberg et al. 2015; Bullock & Boylan-Kolchin 2017), in this work we are interested on a different approach that considers dark matter as a Bose-condensed scalar field. According to this proposal, which has a long history (Baldeschi et al. 1983; Khlopov et al. 1985; Colpi et al. 1986; Sin 1994; Lee & Koh 1996; Guzmán & Matos 2000; Sahni & Wang 2000; Hu et al. 2000; Matos & Ureña-López 2001; Silverman & Mallett 2002; Robles & Matos 2013; Berezhiani & Khoury 2015; Li et al. 2017; Deng et al. 2018; Chavanis 2019a,b; Berezhiani et al. 2021), a system of non-

relativistic scalar particles characterized by a cosmologically large de Broglie wavelength occupy their lowest energy state forming a Bose–Einstein condensate (BEC) that can be described in terms of a coherent wave function Ψ . Such a system behaves as a quantum fluid whose pressure induces a non-zero Jeans scale that can help solve the small-scale problems of the CDM model by suppressing the excess of substructure and producing cored density profiles (Sahni & Wang 2000; Hu et al. 2000). Indeed, a BEC has non-zero pressure even at zero temperature. In particular, the quantum pressure, which has its origin in the uncertainty principle, always contributes. This component is a direct manifestation of the zero-point motions of the constituent particles. On the other hand, BECs with local interparticle interactions characterized by a coupling constant g have a second component of the form $P = g|\Psi|^2/2$. For condensates with sufficiently large repulsive ($g > 0$) interaction strengths or particle densities $|\Psi|^2$, this contribution may be dominant. When this occurs and the quantum pressure becomes negligible against interparticle interactions the system enters the Thomas–Fermi (TF) regime. Self-gravitating BECs with negligible (Hu et al. 2000), dominant (Goodman 2000; Böhmer & Harko 2007) and arbitrary short-range interparticle interactions (Chavanis 2011; Chavanis & Delfini 2011; Lora et al. 2012) have been considered as possible candidates for dark matter haloes.

More recently, motivated by high-resolution cosmological simulations based on the Schrödinger–Poisson equations (Schive et al. 2014a,b; Mocz et al. 2019), attention has focused mainly on axion-like dark matter particles with negligible (attractive) self-interactions (Marsh & Silk 2014; Hlozek et al. 2015; Guth et al. 2015; Marsh 2016; Hui et al. 2017; Bar et al. 2018, 2019; Robles et al. 2018; Bar-Or et al. 2019; Safarzadeh & Spergel 2020; Ferreira 2021; Li et al. 2021;

Hui 2021; Hayashi et al. 2021; Chen et al. 2021). These simulations have confirmed that an axionlike particle with $m \approx 10^{-22} \text{ eV c}^{-2}$ can help solve the small-scale problems of the CDM model while maintaining its successful large-scale predictions. In particular, they show a clear suppression of substructure below $\sim 10^8 M_\odot$ and predict cored haloes with a granular structure dominated by a central *soliton* (whose radius scales inversely with its mass) surrounded by an outer density profile that mimics a Navarro–Frenk–White (NFW) profile (Navarro et al. 1997).

Other numerical estimates based on axionlike particles with no self-interactions lead to values for the mass of dark matter particles that, in general, are consistent with the above result (Lora et al. 2012; Marsh & Pop 2015; Calabrese & Spergel 2016; Schive et al. 2016; Chen et al. 2017; Ureña López et al. 2017; Church et al. 2019). However, the suppression of small-scale structure that such a light mass would induce seem to be in tension with observations of the Lyman- α forest, which rule out boson masses $m \lesssim 10^{-21} \text{ eV c}^{-2}$ (Hui et al. 2017; Iršič et al. 2017; Armengaud et al. 2017; Rogers & Peiris 2021). Nevertheless, this issue is still under debate. There is some consensus that a value of $m \sim 10^{-22} \text{ eV c}^{-2}$ provides the most relevant cosmological consequences and it has been suggested that perhaps more sophisticated models of reionization could alleviate this tension (Hui et al. 2017; Broadhurst et al. 2020; Pozo et al. 2021).

In this work, we assume dark matter to be a self-gravitating BEC consisting of non-relativistic ultralight scalar particles with competing gravitational and short-range repulsive interparticle interactions and investigate the observational implications of such model. Self-gravitating BECs with arbitrary short-range repulsive or attractive self-interactions has been thoroughly studied by Chavanis (2011); Chavanis & Delfini (2011); Chavanis (2021) (for other works concerning repulsive self-interactions, see also Robles & Matos 2012; Suárez & Chavanis 2017; Bernal et al. 2018; Padilla et al. 2021; Dawoodbhoy et al. 2021; Shapiro et al. 2022).

The system is unstable to the formation of stationary self-bound structures that minimize the energy functional. These are the smallest possible gravitationally bound dark matter structures, which we will refer to as *cosmological superfluid droplets*. Guided by recent numerical simulations (Schive et al. 2014a,b; Schwabe et al. 2016; Veltmaat & Niemeyer 2016; Mocz et al. 2017), we assume a hierarchical structure formation with cored dark matter haloes growing around these primordial stationary droplets. With this assumption the model predicts rotation curves that obey a single universal equation in the inner region. A simultaneous fit to a selection of galaxies from the SPARC database (Lelli et al. 2016; Li et al. 2020) chosen with the sole criterion of being strongly dark matter dominated even in the innermost region indicates that the observational data are consistent with the presence of a BEC of ultralight scalar particles of mass $m \approx 2.2 \times 10^{-22} \text{ eV c}^{-2}$ and repulsive contact interactions characterized by a s-wave scattering length $a_s \approx 7.8 \times 10^{-77} \text{ m}$. This result follows from Fig. 1, which will be considered in more detail below. While most of the recent theoretical and numerical works have focused on axionlike dark matter particles with negligible (attractive) self-interactions ($a_s = 0$), the effects of the above small repulsive self-interactions turn out to be essential on cosmological scales. They induce a natural minimum scale length for the size of (non-linear) dark matter structures that, in particular, makes all superfluid droplets have a similar length ($\sim 1 \text{ kpc}$) and contributes to lower the central densities of massive haloes, which may help to solve the small-scale problems of the CDM model.

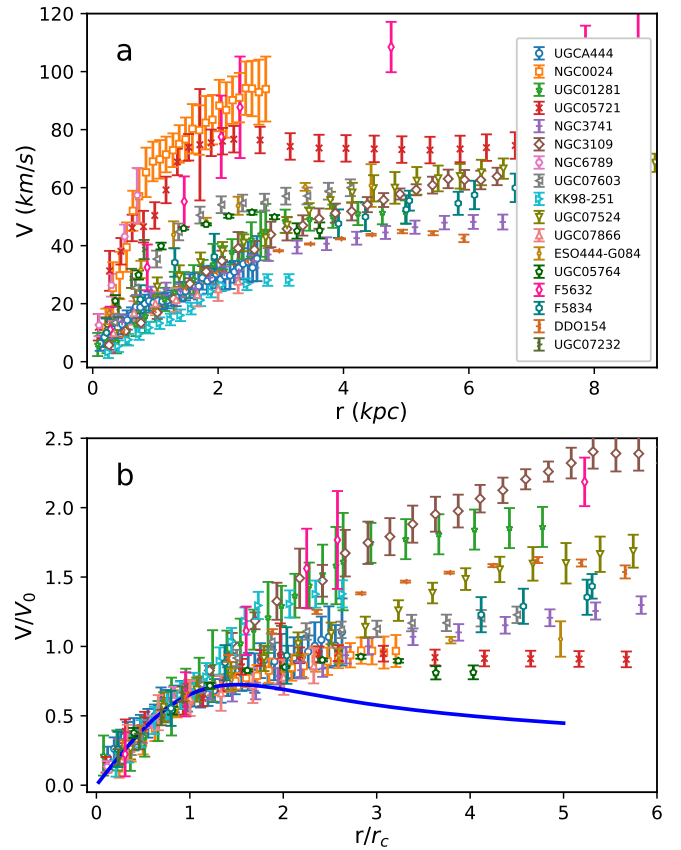


Figure 1. Symbols correspond to the observed dark matter rotation curves of the most dark matter dominated galaxies in the SPARC database. In the top panel velocities and radii are in physical units. In the bottom panel velocities are in units of $V_0 = \sqrt{GM/r_c}$ and radii in units of r_c . This figure shows that within the range of applicability of the theoretical model (for $r \lesssim r_c \sim 1 \text{ kpc}$) the observational data can be well fitted by the universal rotation curve (14) (solid blue line).

2 SELF-INTERACTING BEC DARK MATTER

A dark matter particle of mass $m \sim 10^{-22} \text{ eV c}^{-2}$ and velocity $v \sim 100 \text{ km s}^{-1}$ (Herzog-Arbeitman et al. 2018) has a de Broglie wavelength $\lambda_{\text{dB}} = h/mv \sim 1.2 \text{ kpc}$. This wavelength greatly exceeds the interparticle separation $\bar{n}^{-1/3}$ (where \bar{n} is the average particle-number density), which for typical galactic matter densities $\rho \sim 1 \text{ GeV c}^{-2} \text{ cm}^{-3}$ is of the order $\bar{n}^{-1/3} \sim 10^{-10} \text{ cm}$. Under these conditions, dark matter is deep in the quantum degenerate regime ($\lambda_{\text{dB}} \bar{n}^{1/3} \gg 1$) and must be in the form of a BEC. From the success of the Gross–Pitaevskii equation in reproducing the outcomes of laboratory experiments with ultracold gases, it is now a well-established fact that this equation provides an accurate description of the dynamics of zero-temperature BECs in the mean field regime (see e.g. Muñoz Mateo & Delgado 2006; Huhtamäki et al. 2006). For non-relativistic self-gravitating BECs, it takes the form

$$i\hbar \frac{\partial}{\partial t} \Psi = \left(-\frac{\hbar^2}{2m} \nabla^2 + g |\Psi|^2 + m \Phi_G \right) \Psi, \quad (1)$$

where the strength of the short-range interparticle interactions, $g = 4\pi\hbar^2 a_s/m$, is determined by the s-wave scattering length a_s , and Φ_G is the gravitational potential that satisfies the Poisson equation:

$$\nabla^2 \Phi_G = 4\pi G \rho, \quad (2)$$

where $\rho(\mathbf{r}, t) \equiv m|\Psi(\mathbf{r}, t)|^2$ is the condensate mass density. The ground-state solutions of the dark matter field (cosmological quantum droplets) are localized, self-bound stationary solutions of the coupled Gross–Pitaevskii–Poisson (GPP) equations above that can be found by writing the order parameter in the form $\Psi(\mathbf{r}, t) = \exp(-i\mu_c t/\hbar)\psi(\mathbf{r})$, where μ_c is the chemical potential and ψ satisfies the time-independent equation

$$\mu_c \psi = \left(-\frac{\hbar^2}{2m} \nabla^2 + gn + m\Phi_G \right) \psi, \quad (3)$$

where $n(\mathbf{r}, t) \equiv |\Psi(\mathbf{r}, t)|^2$ is the particle-number density of the condensate. Solving equation (3) is equivalent to finding the critical points of the energy functional

$$E[\psi] = \int d\mathbf{r} \left[\frac{\hbar^2}{2m} |\nabla\psi|^2 + \frac{1}{2}gn^2 + \frac{1}{2}mn\Phi_G \right]. \quad (4)$$

Depending on the total mass $M = m \int d\mathbf{r} |\psi|^2$ and the interaction strength g , the ground-state isotropic dark matter droplets can evolve from (bright) matter-wave solitons to TF-like quantum droplets, with a smooth crossover between the two regimes. In the former case, the system is stabilized by a precise balance between gravitational interactions and quantum pressure, while in the latter the gravitational interaction is counterbalanced by repulsive interparticle interactions. These solutions are well described by a variational Gaussian ansatz (Chavanis 2011):

$$\psi(\mathbf{r}) = \sqrt{\frac{M/m}{(\sqrt{\pi}r_c)^3}} \exp\left(-\frac{r^2}{2r_c^2}\right), \quad (5)$$

where r_c is a characteristic radius to be determined by minimizing the energy functional (4).

Substituting (5) in (4), the total energy as a function of the variational parameter r_c reads

$$E = \frac{3\hbar^2 M}{4m^2 r_c^2} + \frac{gM^2}{\sqrt{32}\pi^3 m^2 r_c^3} - \frac{GM^2}{\sqrt{2}\pi r_c}, \quad (6)$$

where the terms on the right hand side are the contributions from the kinetic E_k , contact self-interaction E_{int} , and gravitational E_G energies, respectively. Minimizing equation (6) with respect to r_c , one obtains the virial relation $2E_k + 3E_{\text{int}} + E_G = 0$, which can be used to eliminate the contact-interaction term and rewrite the energy $E = (E_k + 2E_G)/3$ of the dark matter droplet as

$$E = \frac{\hbar^2 M}{4m^2 r_c^2} - \sqrt{\frac{2}{9\pi}} \frac{GM^2}{r_c}. \quad (7)$$

In order for this energy to be negative the radius r_c must satisfy $r_c \geq \sqrt{9\pi/32} \xi_G \approx \xi_G$, where

$$\xi_G = \frac{\hbar^2}{GMm^2}. \quad (8)$$

The equality, $r_c \approx \xi_G$, occurs for gravitational solitons. Indeed, as can be seen from equation (6), dark matter droplets with r_c of the order of ξ_G can fully balance the gravitational interaction with solely their (zero-point) kinetic energy. By analogy with atomic BECs we call ξ_G *gravitational coherence length*. For $r_c \gg \xi_G$ the contribution of the kinetic energy E_k becomes always negligible against E_G , so that dark matter solitons must necessarily have a radius of the order of ξ_G .

From equation (8) it is clear that the physical size of these solitons depends on their mass and scales as M^{-1} . In the absence of short-range interactions ($a_s = 0$) this would allow the existence of small-sized solitons with a very large mass and density (which scales as

M^4). Repulsive contact interactions ($a_s > 0$) has the desirable effect of introducing an upper limit \mathfrak{M} for the mass of a soliton

$$\mathfrak{M} = \hbar \sqrt{\frac{3\pi}{8Gma_s}}. \quad (9)$$

Indeed, it follows from equation (6) that for dark matter droplets of mass M and radius $r_c \approx \xi_G$, the contribution of the quantum pressure becomes negligible against the contact-interaction energy E_{int} whenever $M^2 \gg \mathfrak{M}^2$. Repulsive contact self-interactions also induce a lower bound for the length scale of gravitational solitons of the order of

$$\mathfrak{R} = \hbar \sqrt{\frac{a_s}{Gm^3}} \approx \xi_G(\mathfrak{M}). \quad (10)$$

In the limit $M^2 \gg \mathfrak{M}^2$, when the quantum pressure becomes negligible, the dark matter droplets lose their solitonic character and evolve into TF-like droplets stabilized only by the repulsive interparticle interactions. As follows from equation (6), these TF-like droplets have a radius of the order of \mathfrak{R} (hence, independent of the mass M) and, unlike the case of gravitational solitons, their densities only grow linearly with M . Thus, the parameter \mathfrak{R} determines the length scale of the smallest gravitationally bound dark matter structures. The inclusion in the model of short-range interparticle interactions naturally induce a small-scale cut-off dependent only on the microscopic parameters of the condensate.

Minimization of the energy functional gives the radii of the superfluid dark matter droplets (Chavanis 2011), which we conveniently write in the form

$$r_c = \sqrt{9\pi/8} \left(1 + \sqrt{1 + (M/\mathfrak{M})^2} \right) \xi_G. \quad (11)$$

In the solitonic regime ($M^2 \ll \mathfrak{M}^2$), when local self-interactions can be neglected, equation (11) reduces to $r_c \approx \sqrt{9\pi/2} \xi_G$, while in the TF regime ($M^2 \gg \mathfrak{M}^2$), when the quantum pressure is negligible (Goodman 2000; Böhmer & Harko 2007), $r_c \approx \sqrt{3} \mathfrak{R}$. The parameter \mathfrak{M}^2 determines the crossover between the two regimes.

3 STATIONARY DARK MATTER DROPLETS. UNIVERSAL MASS PROFILE AND ROTATION CURVE

Stationary dark matter droplets are fully characterized by the condensate wave function (5) with r_c given by equation (11). Only two parameters are required to describe the fundamental properties of the Bose–Einstein condensate, namely, the boson mass m and the s -wave scattering length a_s that determines the strength of interparticle interactions. Once these parameters are known, the total mass M is sufficient to completely specify a given dark matter droplet. Remarkably, these superfluid dark matter droplets exhibit a *universal mass profile*. Indeed, the enclosed mass within radius r , which is given by

$$M(r) = m \int_0^r d\mathbf{r} |\psi|^2, \quad (12)$$

when expressed in units of the total mass M and as a function of the dimensionless radius $x = r/r_c$, satisfies the following universal mass profile:

$$M_{\text{DM}}(x) = \text{erf}(x) - 2\pi^{-\frac{1}{2}} x \exp(-x^2). \quad (13)$$

The corresponding rotation curve was obtained by Chavanis (2011). In view of equation (13), in this work we find it most convenient for our purposes to rewrite the expression derived by Chavanis (2011) in terms of convenient dimensionless quantities. Indeed, in

units of the characteristic circular velocity $V_0 = \sqrt{GM/r_c}$, the rotation curves of the dark matter droplets as a function of $x = r/r_c$ obey the *universal equation*

$$V_{\text{DM}}(x) = \sqrt{x^{-1} M_{\text{DM}}(x)} = \sqrt{x^{-1} \text{erf}(x) - 2\pi^{-\frac{1}{2}} \exp(-x^2)}. \quad (14)$$

Thus the present model, which considers dark matter to be a superfluid Bose–Einstein condensate of ultralight scalar particles with short-range repulsive interparticle interactions, predicts a universal mass profile and a corresponding universal rotation curve in the inner region ($r \lesssim r_c$) of dark-matter dominated galactic haloes. In what follows, we aim to elucidate whether the observational data are consistent with these theoretical predictions.

4 OBSERVATIONAL IMPLICATIONS

We assume a hierarchical structure formation scenario where, under the combined action of gravity and emergent effective phase-dependent interactions, granular dark matter haloes grow around the above quantum droplets, which we assume survive as stationary solutions of the GPP equations at the centres of the haloes. As already mentioned, this assumption seems to be well supported by recent numerical simulations (Schive et al. 2014a,b; Schwabe et al. 2016; Veltmaat & Niemeyer 2016; Mocz et al. 2017).

On the other hand, we will also assume that the model is applicable, to a good approximation, *at least* up to a radius $r_{\text{F}} = 1.2$ kpc. Although the latter assumption is mainly motivated by the need to have sufficient data resolution in the region of interest and can, in fact, be relaxed somewhat (see Appendix A), it also seems to be a reasonable assumption (see e.g. Schive et al. 2014a; Hui et al. 2017).

The actual range of applicability of the model corresponds to the region where the theoretical curve is able to adequately account for the observational data and, for a given galactic halo, can be written, in general, as $r \lesssim \alpha r_c \sim r_c$, where α is an unknown parameter of order unity and r_c is the radius of the central quantum droplet. As we will see, for all the galaxies considered in this work r_c turns out to be of the order of 1 kpc. However, this value is not known a priori, a fact that has determined our fitting strategy (see Appendix A for details).

We stress that in this work we have pursued minimal model dependence. In fact, our model relies solely on the above two assumptions. With these hypotheses the model predicts observational rotation curves that must satisfy the universal equation (14) in the inner region of the galactic haloes (for a previous phenomenological construction of a universal rotation curve see Persic et al. 1996; Karukes & Salucci 2016). Since the presence of baryonic matter can significantly modify the dark matter distribution in the centre of the haloes, for the above assumption to be true baryonic matter should be negligible even in this region. Indeed, equation (14) was obtained under the assumption of a negligible contribution of baryonic matter, which accordingly was not considered in the coupled GPP equations. If this were not the case, there is no reason to believe that equation (14) remains true, and the corresponding GPP equations would have to be solved numerically. Therefore, the application of the above analytical formulation to the innermost regions of DM haloes requires galaxies with a negligible contribution of baryonic matter even in this central region.

It is worth mentioning that our model assumes stationary cores located at the centre of the haloes, and does not consider the possible random motion around this position [as pointed out for solitonic cores by Chowdhury et al. (2021)], which, if effective, could also be a source of additional uncertainty in the resulting best-fit parameters.

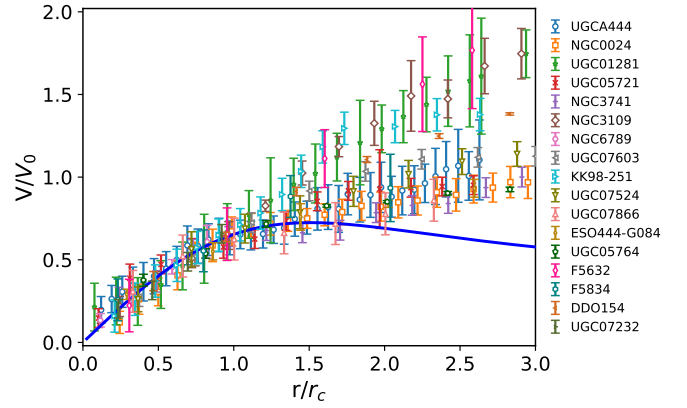


Figure 2. This figure is a zoom-in of Fig. 1b. Symbols correspond to the observed dark matter rotation curves of the most dark matter dominated galaxies in the SPARC database (see legend). Velocities are in units of $V_0 = \sqrt{GM/r_c}$ and radii in units of r_c . The figure shows that within the range of applicability of the theoretical model (for $r \lesssim r_c \sim 1$ kpc) the observational data can be well fitted by the universal rotation curve (14) (solid blue curve).

To confront the model with observations, we use the SPARC database restricting our analysis to high-quality rotation curves with quality flag $Q = 1$ or 2 (Lelli et al. 2016; Li et al. 2020). This database provides the observed circular velocities V_{obs} of 175 late-type galaxies along with the contributions from gas V_{gas} and stars (disk and bulge) V_* , so that the dark matter contribution can be inferred from the relation $V_{\text{obs}}^2 = V_{\text{DM}}^2 + V_{\text{gas}}^2 + Y_* V_*^2$ (see Lelli et al. (2016); Li et al. (2020) for details). We focus on galaxies that are strongly dominated by dark matter even within $r \lesssim 1$ kpc and that are well resolved in this region. This excludes galaxies with bulges, since baryonic matter always has a significant contribution in the innermost region of these galaxies. We then calculate the dark matter contribution to the rotation curves (V_{DM}) of the remaining galaxies using the relation above with a constant stellar mass-to-light ratio $Y_* = 0.47 M_{\odot}/L_{\odot}$ (McGaugh & Schombert 2014; Lelli et al. 2016) and carefully analyse the different contributions in the region of interest ($r \lesssim 1$ kpc). Restricting ourselves to galaxies with a ratio $V_{\text{DM}}/V_{\text{obs}} > 0.75$ at virtually all points in this region, we are finally left with 17 bulgeless galaxies. Figure 1a shows the dark matter contribution to the rotation curves of these galaxies. As is apparent, the sample covers quite different curve slopes and maximum circular velocities (ranging from ~ 30 to 100 km s^{-1}), so that, despite observational uncertainties, a simultaneous fit of the 17 curves in the sample with the predicted universal rotation curve (14) imposes a stringent constraint on the parameters of the model. Figure 1b shows the result of such a fit. As fitting parameters we have used m , a_s and the different total masses M_i of the dark matter droplets residing at the centre of each galaxy and have implemented a Maximum Likelihood fitting method that minimizes the standard χ^2 function $\sum (V_{\text{DM}}^{\text{obs}} - V_{\text{DM}}^{\text{theo}})^2 / (\Delta V_{\text{DM}}^{\text{obs}})^2$, where $V_{\text{DM}}^{\text{obs}}$ is the dark matter contribution to the observed rotation velocity, $\Delta V_{\text{DM}}^{\text{obs}}$ is its observational uncertainty and $V_{\text{DM}}^{\text{theo}}$ is the theoretical prediction (14).

As the model is only applicable in the inner region of the haloes, in fitting the observational data we have only considered rotation velocities corresponding to radii $r \leq 1.2$ kpc. On the other hand, since the galaxies in the sample have very different spatial resolutions in this region, we have limited the maximum number of points to fit per galaxy to 6 to avoid overweighting some galaxies too much. The best-fit parameters (maximum likelihood) are collected in Table A1. In

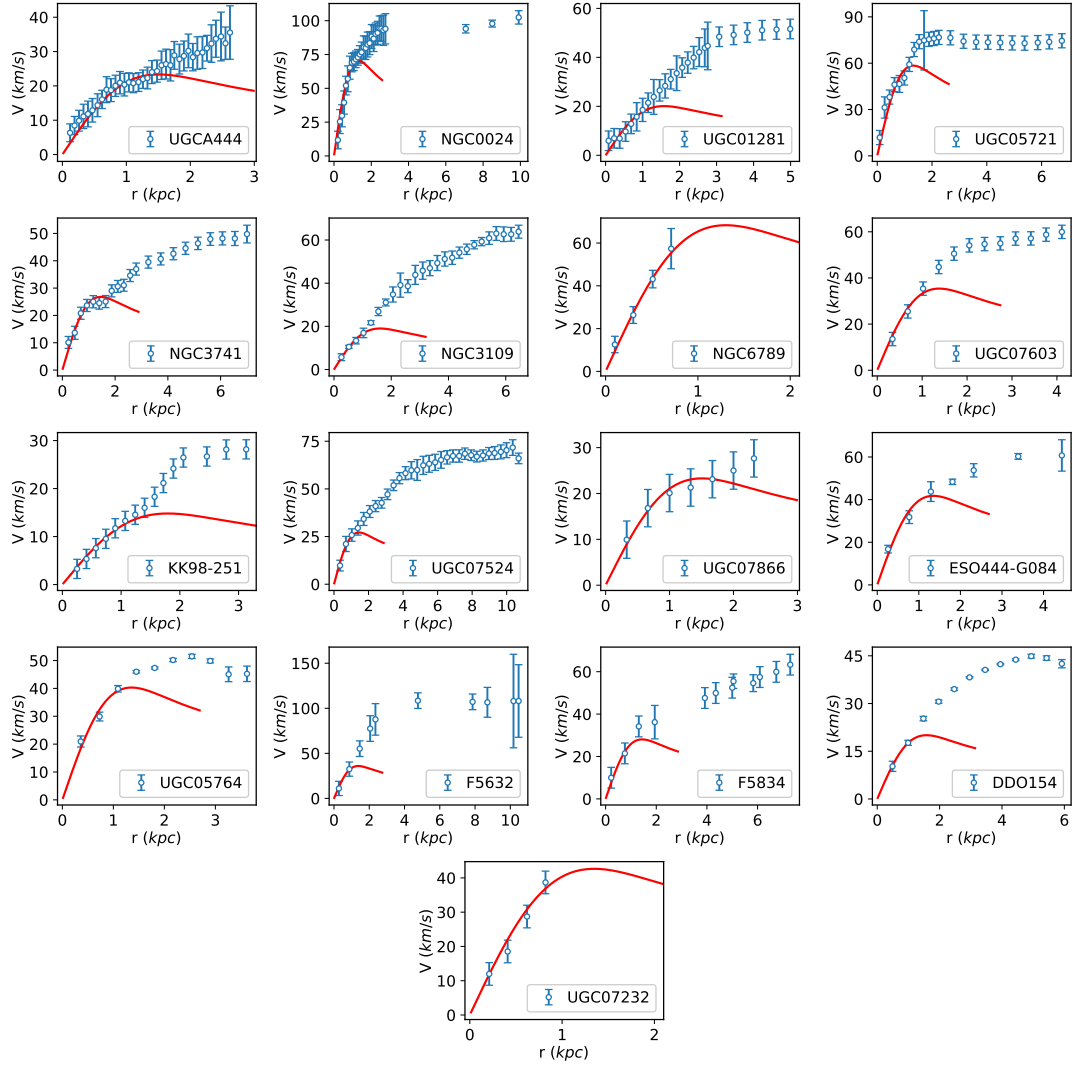


Figure 3. Same rotation curves as in Fig. 2 but in physical units (velocities in km s^{-1} and radii in kpc). Solid red lines are the fits with the universal rotation curve (14).

this table we also show the radius r_c of the halo cores, obtained from equation (11), as well as the masses of the halo cores $M_c \equiv M(r_c) \simeq 0.43 M$, which follow from the definition (12) of the enclosed mass within radius r_c (see also Fig. A1). Table A1 also gives the enclosed masses within the innermost 300 pc, M_{300} , and the corresponding mean densities, ρ_{300} .

Figure 1b shows that within the range of applicability of the theoretical model (for $r \lesssim r_c \sim 1$ kpc) the observational data can be well fitted by the universal rotation curve (14) predicted by the self-interacting BEC model (solid blue curve). See also Figs. 2 and 3. Figure 2 is a zoom-in of Fig. 1b while Fig. 3 shows what the universal rotation curve looks like for each individual galaxy in physical units (velocities in km s^{-1} and radii in kpc). The good agreement between theoretical predictions and observations indicates that the observational rotation curves are consistent with the presence of a superfluid dark matter droplet residing at the centre of galactic haloes and consisting of ultralight scalar particles of mass $m \simeq 2.2 \times 10^{-22} \text{ eV c}^{-2}$ and repulsive contact interactions characterized by a s-wave scattering length $a_s \simeq 7.8 \times 10^{-77} \text{ m}$. For these parameters, we have

$$\mathfrak{M} = 4 \times 10^7 M_\odot, \quad \mathfrak{R} = 487 \text{ pc}. \quad (15)$$

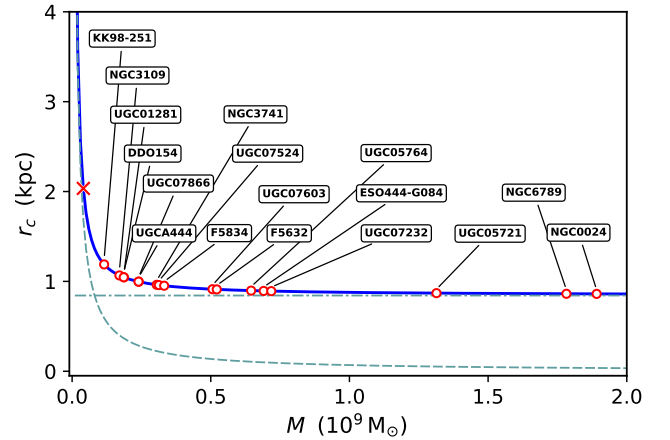


Figure 4. Location of galaxies (open circles) in the r_c – M parameter space. The solid line corresponds to equation (11), while the dashed and dot-dashed lines correspond, respectively, to the solitonic and TF regimes. The cross symbol marks the location of a dark matter droplet of mass \mathfrak{M} . As can be seen, the cores of all galaxies in the sample are either in the TF or in the crossover regime, with radii ~ 1 kpc.

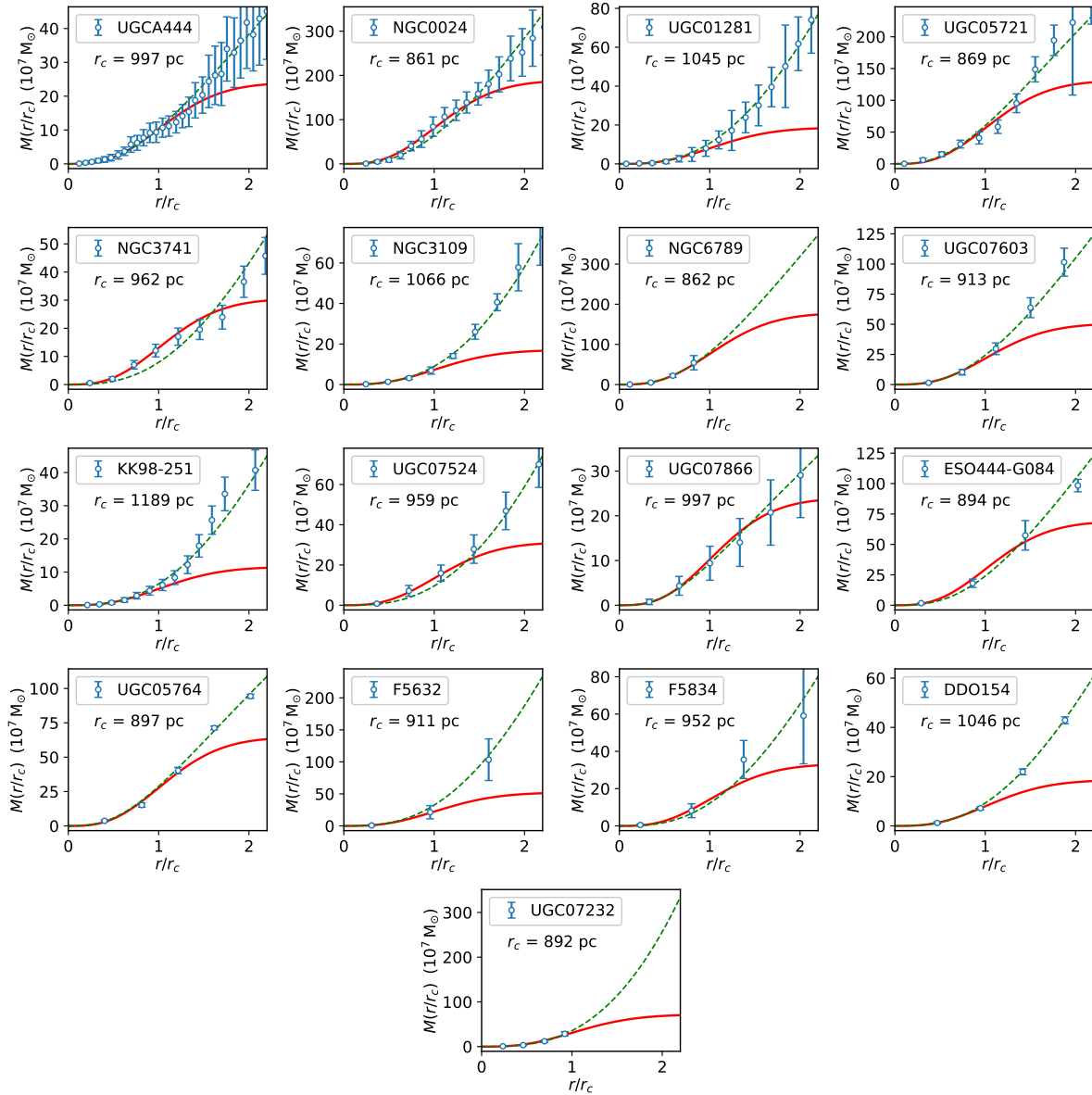


Figure 5. Dark matter mass enclosed within radius r/r_c . Open symbols correspond to the observational data, dashed green lines are fits with the Burkert model and solid red lines are fits with the enclosed mass predicted by equation (13). Note that if we had expressed the enclosed masses in units of M we would have obtained a single universal mass profile within $r \lesssim r_c \sim 1$ kpc. In fact, this figure contains essentially the same information as Figs. 2 and 3. While the total masses M of the superfluid quantum droplets residing at the halo centres are, in general, not observable, the above plots show that the mass profiles resulting from them are not only consistent with the observed data but, in general, within the range of applicability of the model ($r \lesssim r_c$) fit them better than Burkert’s phenomenological model.

Figure 4 shows the location of each galaxy (open circles) in the r_c – M parameter space. The solid line corresponds to equation (11), while the dashed and dot-dashed lines correspond, respectively, to the solitonic and TF regimes. The latter, characterized by a constant radius, $r_c \approx \sqrt{3} \mathfrak{R} = 843$ pc, determines the minimum length scale of any dark matter structure. The cross symbol marks the location of a dark matter droplet of mass \mathfrak{M} . Droplets with mass $M > \mathfrak{M}$ and radius $r_c < r_c(\mathfrak{M}) \approx 2$ kpc are not supported by quantum zero-point motions (quantum pressure) and cannot be considered to be solitons. As can be seen, the cores of all galaxies in the sample are either in the TF regime or in the crossover between the two regimes, with radii ~ 1 kpc, ranging from 861 pc (for NGC0024) to 1189 pc (for KK98–251) and corresponding masses ranging from $1.9 \times 10^9 M_\odot$

to $1.2 \times 10^8 M_\odot$, respectively. Note that those galaxies whose cores are in the TF regime could also be described analytically by an alternative formulation to equation (5) (see e.g. Goodman 2000; Böhmer & Harko 2007). However, our formulation provides a richer scenario, as it can account for the smooth transition between the solitonic and TF regimes.

In Fig. 5 we show that, in general, within the range of applicability of the model ($r \lesssim r_c$), the universal mass profile implied by the above masses fits the observational data better than Burkert’s phenomenological model (Burkert 1995). On the other hand, the mass contained within $r < 300$ pc varies between $5.6 \times 10^7 M_\odot$ (NGC0024) and $1.3 \times 10^6 M_\odot$ (KK98–251) with a mean value of $1.6 \times 10^7 M_\odot$ and mean density $0.14 M_\odot/\text{pc}^3$, results that are in

good agreement with typical values observed in the most dark matter dominated galaxies in the Local Group (Gilmore et al. 2007; Strigari et al. 2008). Note that our results for m and a_s are consistent with those corresponding to what was called BECT model by Chavanis (2021). However, according to our results (see Fig. 4), for a given pair (m, a_s) dark matter droplets can be in different regimes depending on their masses M .

5 CONCLUSIONS

Despite the undeniable success of the standard CDM model on large scales, this model can hardly explain the observed mass profiles at the centres of galactic haloes. Motivated by the small-scale problems of the CDM model, in this work we have considered dark matter to be a quantum fluid in the form of a self-gravitating Bose–Einstein condensate consisting of non-relativistic ultralight scalar particles with competing gravitational and repulsive contact interactions characterized by a s-wave scattering length $a_s \geq 0$. This quantum system, governed by a cosmologically large coherent wave function Ψ , is unstable to the formation of stationary self-bound cosmological droplets that minimize the energy functional and constitute the smallest possible gravitationally bound dark matter structures. We have shown that these superfluid dark matter droplets exhibit a universal mass profile and a corresponding universal rotation curve. We have also assumed a hierarchical structure formation scenario with granular dark matter haloes growing around these primordial stationary droplets, which survive at the centres of the haloes. With this hypothesis the model predicts cored dark matter haloes that must satisfy a universal mass profile and a universal rotation curve in the inner region ($r \lesssim r_c$).

To elucidate whether these theoretical predictions are consistent with the observational data, we have simultaneously fitted the observed rotation curves of the most dark matter dominated galaxies in the SPARC database with the predicted universal rotation curve (14) using as free parameters the mass m and scattering length a_s of the constituent bosons and the total mass M of the dark matter quantum droplets residing at the centre of each halo.

Although there are other works in the literature that fit galaxies from the SPARC database (see e.g. Bernal et al. 2018; Kendall & Easther 2020), they are restricted to axionlike dark matter particles with no self-interactions or are based on theoretical models that have not allowed to constrain the properties of the dark matter particle. On the other hand, much of this work relies on the core-halo relation (Schive et al. 2014b), the validity of which has not yet been fully confirmed (see e.g. Kendall & Easther 2020). In contrast, in the present work we have sought minimal model dependence. Our model relies on only two assumptions: i) dark matter dominated galactic cores are well described by a stationary state of the GPP equations and, ii) the model is applicable at least up to a radius $r_F = 1.2$ kpc.

Our approach takes advantage of the predicted universal character of the mass profiles and corresponding rotation curves in the innermost region of the most dark matter dominated haloes to simultaneously fit the observational data of all galaxies in the sample, thus increasing their statistical significance. In this way, we have been able to demonstrate remarkable agreement between observations and theoretical predictions and have obtained precise estimates for both the mass m and the scattering length a_s of dark matter particles. To our knowledge, this is the first time that a precise estimate of a_s has been inferred from observational data (rather than a wide range of possible values, spanning many orders of magnitude), as well as the first evidence, based on a motivated theoretical model, for universal properties of the mass profiles at the centres of galactic haloes.

Our best-fit results indicate that observational data are consistent with the existence of self-gravitating superfluid dark matter droplets in the centres of the haloes that satisfy a universal rotation curve and consist of ultralight scalar particles with very weak repulsive local self-interactions. Despite the small value of the scattering length, $a_s \sim 10^{-76}$ m, these self-interactions have profound consequences on cosmological scales. Unlike the case of ultralight axionlike pseudoscalar particles with negligible (attractive) self-interactions ($a_s = 0$), which necessarily predict solitons at the centres of the haloes with a radius and density that scales as M^{-1} and M^4 , respectively, a small repulsive self-interaction induces a natural minimum scale length for the size of (non-linear) dark matter structures and favours central superfluid dark matter droplets that lie in either the Thomas–Fermi or the crossover regimes, having an essentially constant radius $r_c \sim 1$ kpc and a shallow density that scales as M . This can help solve the small-scale problems of the CDM model. Note that since the theoretical lower limit for M is of the order of the Jeans mass $M_J \approx 1 \times 10^7 M_\odot$, there is still room in the self-interacting model for the existence of quasi-solitons with maximum radii smaller than $r_c(M_J) \approx 7$ kpc.

Since for distances much larger than $\lambda_{dB} \sim 1$ kpc both solitons and TF-like droplets behave essentially like CDM particles with mass $\rho \lambda_{dB}^3$ (Schive et al. 2014a; Hui et al. 2017), on large scales the self-interacting BEC dark matter model becomes virtually indistinguishable from the standard CDM model. Therefore, in order to corroborate our results it would be interesting to probe the cores of the most dark matter dominated galaxies with higher resolution, as well as to carry out numerical simulations to check the model beyond the inner part of the haloes (where an analytical treatment is applicable) or in the presence of a non-negligible baryonic contribution. We hope that our results will stimulate further investigations in these directions.

ACKNOWLEDGEMENTS

We thank J. E. Betancort-Rijo and C. Dalla Vecchia for stimulating discussions. V. D. acknowledges support from Agencia Estatal de Investigación (Ministerio de Ciencia e Innovación, Spain) and Fondo Europeo de Desarrollo Regional (FEDER, EU) under Grants PID2019-105225GB-I00 and FIS2016-79596-P.

DATA AVAILABILITY

The data underlying this article will be shared on reasonable request to the corresponding author.

REFERENCES

- Armengaud E., Palanque-Delabrouille N., Yèche C., Marsh D. J. E., Baur J., 2017, *Mon. Not. R. Astron. Soc.*, 471, 4606
- Baldeschi M., Gelmini G., Ruffini R., 1983, *Physics Letters B*, 122, 221
- Bar-Or B., Fouvy J. B., Tremaine S., 2019, *The Astrophysical Journal*, 871, 28
- Bar N., Blas D., Blum K., Sibiryakov S., 2018, *Phys. Rev. D*, 98, 083027
- Bar N., Blum K., Eby J., Sato R., 2019, *Phys. Rev. D*, 99, 103020
- Berezhiani L., Khoury J., 2015, *Phys. Rev. D*, 92, 103510
- Berezhiani L., Cintia G., Warkentin M., 2021, *Phys. Lett. B*, 819, 136422
- Bernal T., Fernández-Hernández L. M., Matos T., Rodríguez-Meza M. A., 2018, *Mon. Not. R. Astron. Soc.*, 475, 1447
- Böhmer C. G., Harko T., 2007, *J. Cosmol. Astropart. Phys.*, 2007, 025

- Boylan-Kolchin M., Bullock J. S., Kaplinghat M., 2011, *Mon. Not. R. Astron. Soc.*, 415, L40
- Broadhurst T., de Martino I., Luu H. N., Smoot G. F., Tye S.-H. H., 2020, *Phys. Rev. D*, 101, 083012
- Bullock J. S., Boylan-Kolchin M., 2017, *Annual Review of Astronomy and Astrophysics*, 55, 343
- Burkert A., 1995, *The Astrophysical Journal*, 447, L25
- Calabrese E., Spergel D. N., 2016, *Mon. Not. R. Astron. Soc.*, 460, 4397
- Chavanis P. H., 2011, *Phys. Rev. D*, 84, 043531
- Chavanis P. H., 2019a, *Phys. Rev. D*, 100, 083022
- Chavanis P. H., 2019b, *Phys. Rev. D*, 100, 123506
- Chavanis P. H., 2021, *Phys. Rev. D*, 103, 123551
- Chavanis P. H., Delfini L., 2011, *Phys. Rev. D*, 84, 043532
- Chen S.-R., Schive H.-Y., Chiueh T., 2017, *Mon. Not. R. Astron. Soc.*, 468, 1338
- Chen J., Du X., Lentz E. W., Marsh D. J. E., Niemeyer J. C., 2021, *Phys. Rev. D*, 104, 083022
- Chowdhury D. D., van den Bosch F. C., Robles V. H., van Dokkum P., Schive H.-Y., Chiueh T., Broadhurst T., 2021, *The Astrophysical Journal*, 916, 27
- Church B. V., Mocz P., Ostriker J. P., 2019, *Mon. Not. R. Astron. Soc.*, 485, 2861
- Colpi M., Shapiro S. L., Wasserman I., 1986, *Phys. Rev. Lett.*, 57, 2485
- Dawoodbhoj T., Shapiro P. R., Rindler-Daller T., 2021, *Mon. Not. R. Astron. Soc.*, 506, 2418
- Deng H., Hertzberg M. P., Namjoo M. H., Masoumi A., 2018, *Phys. Rev. D*, 98, 023513
- Ferreira E. G. M., 2021, *Astron. Astrophys. Rev.*, 29, 7
- Flores R. A., Primack J. R., 1994, *The Astrophysical Journal*, 427, L1
- Gilmore G., Wilkinson M. I., Wyse R. F. G., Kleya J. T., Koch A., Evans N. W., Grebel E. K., 2007, *The Astrophysical Journal*, 663, 948
- Goodman J., 2000, *New Astronomy*, 5, 103
- Guth A. H., Hertzberg M. P., Prescod-Weinstein C., 2015, *Phys. Rev. D*, 92, 103513
- Guzmán F. S., Matos T., 2000, *Class. Quantum Grav.*, 17, L9
- Hayashi K., Ferreira E. G. M., Chan H. Y. J., 2021, *The Astrophysical Journal Letters*, 912, L3
- Herzog-Arbeitman J., Lisanti M., Madau P., Necib L., 2018, *Phys. Rev. Lett.*, 120, 041102
- Hlozek R., Grin D., Marsh D. J. E., Ferreira P. G., 2015, *Phys. Rev. D*, 91, 103512
- Hu W., Barkana R., Gruzinov A., 2000, *Phys. Rev. Lett.*, 85, 1158
- Huhtamäki J. A. M., Möttönen M., Isoshima T., Pietilä V., Virtanen S. M. M., 2006, *Phys. Rev. Lett.*, 97, 110406
- Hui L., 2021, *Annu. Rev. Astron. Astrophys.*, 59, 247
- Hui L., Ostriker J. P., Tremaine S., Witten E., 2017, *Phys. Rev. D*, 95, 043541
- Iršič V., Viel M., Haehnelt M. G., Bolton J. S., Becker G. D., 2017, *Phys. Rev. Lett.*, 119, 031302
- Karukes E. V., Salucci P., 2016, *Mon. Not. R. Astron. Soc.*, 465, 4703
- Kauffmann G., White S. D. M., Guiderdoni B., 1993, *Mon. Not. R. Astron. Soc.*, 264, 201
- Kendall E., Easter R., 2020, *Publications of the Astronomical Society of Australia*, 37, e009
- Khlopov M. Y., Malomed B. A., Zeldovich Y. B., 1985, *Mon. Not. R. Astron. Soc.*, 215, 575
- Klypin A., Kravtsov A. V., Valenzuela O., Prada F., 1999, *The Astrophysical Journal*, 522, 82
- Lee J.-W., Koh I.-G., 1996, *Phys. Rev. D*, 53, 2236
- Lelli F., McGaugh S. S., Schombert J. M., 2016, *The Astronomical Journal*, 152, 157
- Li B., Shapiro P. R., Rindler-Daller T., 2017, *Phys. Rev. D*, 96, 063505
- Li P., Lelli F., McGaugh S., Schombert J., 2020, *The Astrophysical Journal Supplement Series*, 247, 31
- Li X., Hui L., Yavetz T. D., 2021, *Phys. Rev. D*, 103, 023508
- Lora V., Magaña J., Bernal A., Sánchez-Salcedo F. J., Grebel E. K., 2012, *J. Cosmol. Astropart. Phys.*, 2012, 011
- Marsh D. J., 2016, *Physics Reports*, 643, 1
- Marsh D. J. E., Pop A. R., 2015, *Mon. Not. R. Astron. Soc.*, 451, 2479
- Marsh D. J. E., Silk J., 2014, *Mon. Not. R. Astron. Soc.*, 437, 2652
- Matos T., Ureña-López L. A., 2001, *Phys. Rev. D*, 63, 063506
- McGaugh S. S., Schombert J. M., 2014, *The Astronomical Journal*, 148, 77
- Mocz P., Vogelsberger M., Robles V. H., Zavala J., Boylan-Kolchin M., Fialkov A., Hernquist L., 2017, *Mon. Not. R. Astron. Soc.*, 471, 4559
- Mocz P., et al., 2019, *Phys. Rev. Lett.*, 123, 141301
- Moore B., 1994, *Nature*, 370, 629
- Moore B., Ghigna S., Governato F., Lake G., Quinn T., Stadel J., Tozzi P., 1999, *The Astrophysical Journal*, 524, L19
- Muñoz Mateo A., Delgado V., 2006, *Phys. Rev. Lett.*, 97, 180409
- Navarro J. F., Frenk C. S., White S. D. M., 1997, *The Astrophysical Journal*, 490, 493
- Padilla L. E., Rindler-Daller T., Shapiro P. R., Matos T., Vázquez J. A., 2021, *Phys. Rev. D*, 103, 063012
- Persic M., Salucci P., Stel F., 1996, *Mon. Not. R. Astron. Soc.*, 281, 27
- Pozo A., Broadhurst T., de Martino I., Luu H. N., Smoot G. F., Lim J., Neyrinck M., 2021, *Mon. Not. R. Astron. Soc.*, 504, 2868
- Robles V. H., Matos T., 2012, *Mon. Not. R. Astron. Soc.*, 422, 282
- Robles V. H., Matos T., 2013, *The Astrophysical Journal*, 763, 19
- Robles V. H., Bullock J. S., Boylan-Kolchin M., 2018, *Mon. Not. R. Astron. Soc.*, 483, 289
- Rogers K. K., Peiris H. V., 2021, *Phys. Rev. Lett.*, 126, 071302
- Safarzadeh M., Spergel D. N., 2020, *The Astrophysical Journal*, 893, 21
- Sahni V., Wang L., 2000, *Phys. Rev. D*, 62, 103517
- Schive H. Y., Chiueh T., Broadhurst T., 2014a, *Nature Phys.*, 10, 496–
- Schive H.-Y., Liao M.-H., Woo T.-P., Wong S.-K., Chiueh T., Broadhurst T., Hwang W.-Y. P., 2014b, *Phys. Rev. Lett.*, 113, 261302
- Schive H.-Y., Chiueh T., Broadhurst T., Huang K.-W., 2016, *The Astrophysical Journal*, 818, 89
- Schwabe B., Niemeyer J. C., Engels J. F., 2016, *Phys. Rev. D*, 94, 043513
- Shapiro P. R., Dawoodbhoj T., Rindler-Daller T., 2022, *Mon. Not. R. Astron. Soc.*, 509, 145
- Silverman M. P., Mallett R. L., 2002, *Gen. Relativ. Gravit.*, 34, 633
- Sin S.-J., 1994, *Phys. Rev. D*, 50, 3650
- Strigari L. E., Bullock J. S., Kaplinghat M., Simon J. D., Geha M., Willman B., Walker M. G., 2008, *Nature*, 454, 1096
- Suárez A., Chavanis P. H., 2017, *Phys. Rev. D*, 95, 063515
- Ureña López L. A., Robles V. H., Matos T., 2017, *Phys. Rev. D*, 96, 043005
- Veltmaat J., Niemeyer J. C., 2016, *Phys. Rev. D*, 94, 123523
- Weinberg D. H., Bullock J. S., Governato F., Kuzio de Naray R., Peter A. H. G., 2015, *Proceedings of the National Academy of Sciences*, 112, 12249

APPENDIX A: FITTING CRITERIA

In this Appendix we will examine in more detail the criteria we have followed in our fitting strategy.

Figure A1 shows the predicted universal mass profile (13) of a dark matter galactic core along with the corresponding universal rotation curve (14). At $x \equiv r/r_c = 1$, where r_c is the radius of the dark matter core given by equation (11), the enclosed mass represents 43% of the total mass and the circular velocity takes the value $V_{\text{DM}} = 0.65$. As can be seen in the figure, the rotation curve attains its maximum, $V_{\text{DM}}^{\text{max}} = 0.72$, at $x = 1.5$, and the enclosed mass within this radius corresponds to 79% of the total mass.

Consider a strongly dark matter dominated galaxy and assume that, as predicted by our model, its observational rotation curve can be well described in the innermost region of the galactic halo by the universal profile (14), up to a certain radius $r_L \approx \alpha r_c$, where r_c is the radius of the central dark matter droplet and α is an unknown factor of order unity. Let us assume for the moment (we will remove this assumption later) that the observational data have negligible uncertainties (error bars). Since the theoretical curve (14) only depends on three independent parameters, it is sufficient to impose that it passes through any three points *within* the radius r_L to properly account for

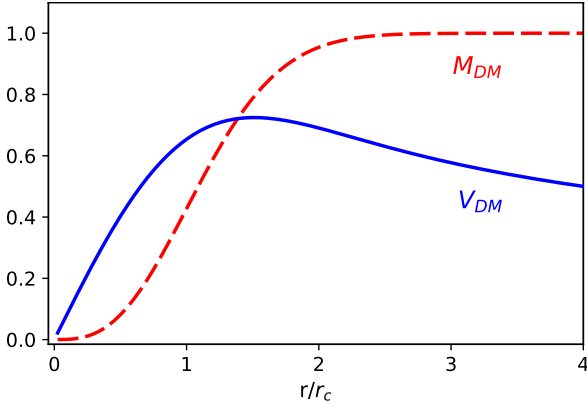


Figure A1. Predicted universal mass profile (13) of a dark matter galactic core (dashed red line) along with the corresponding universal rotation curve (14) (solid blue line).

the whole curve. Thus, in this hypothetical case of accurate observational data, the contribution of any other points, as long as they lie within the radius r_L , should not lead to an appreciable modification of the resulting best-fit parameters of the model. In contrast, by forcing the theoretical curve to pass through points where the model is no longer applicable ($r > r_L$), a significant bias in the inferred parameters can be introduced, and this is true regardless of whether or not the observational data have negligible uncertainties. It is therefore important to prevent observational data beyond the range of applicability of the model from intervening in the fitting procedure. To achieve this, in principle, it would be sufficient to limit the fit to a maximum radius $r_F < r_L$.

However, while the assumptions of the model allow us to ensure that its range of applicability ($r \lesssim \alpha r_c$ with $\alpha \sim O(1)$) is of the order of the radius r_c of the central dark matter droplet, the value of r_c itself is not known a priori. In fact, this value is one of the results of the fit. It is thus clear that some assumption has to be made in order to proceed further. In this work, we assume that the model can be applied to a good approximation *at least* up to a certain radius r_F . In view of the considerations above, the safest and most conservative option to avoid biased results is to take the smallest possible value for r_F . However, in doing so, one must be aware that the uncertainties in the observational data are by no means negligible. In fact, it can be readily verified that due to these uncertainties the fits of two individual galaxies, even within their innermost regions, can lead to quite different model parameters. The easiest way to overcome this difficulty is to increase the size of the sample. As the sample size increases, random uncertainties are expected to cancel out to a greater extent, thus increasing our confidence in the observational data and, hence, in the model predictions.

One way to increase the sample size would be to choose a larger fit radius r_F , however, as mentioned above, this must be done with care to minimise the risk of biased results. Observations and numerical simulations seem to indicate that a reasonable value would be $r_F \sim 1$ kpc. Since most galaxies are poorly resolved in this region, this is far from enough to compensate for observational uncertainties. To further increase the sample size, we have taken advantage of the fact that the model predicts a universal rotation curve in the innermost region of galactic haloes, which allows us to simultaneously fit all 17 galaxies as if they were a single data set. This is a crucial point in our approach. Thus, our fitting strategy consists of reducing the impact of observational uncertainties by increasing the statistical

significance of the sample while minimising the risk of biased results. To this end, we have simultaneously fit all galaxies and have taken the smallest possible fit radius r_F that still allows sufficient resolution in the region of interest. We believe that the best compromise is achieved for $r_F = 1.2$ kpc. The best-fit parameters obtained with this value are collected in Table A1. In particular, the boson mass and the s-wave scattering length are, respectively, $m \simeq 2.2 \times 10^{-22} \text{ eV c}^{-2}$ and $a_s \simeq 7.8 \times 10^{-77} \text{ m}$, while the radii r_c of the central dark matter droplets are all of the order of 1 kpc.

We have also fitted the observational data using $r_F = 1$ and 1.4 kpc. In the first case, we have obtained $m \simeq 1.8 \times 10^{-22} \text{ eV c}^{-2}$ and $a_s \simeq 2.5 \times 10^{-77} \text{ m}$. While this result is in reasonable agreement with the previous one, in this case the number of data points to fit is clearly smaller as some of the galaxies that previously contributed 6 points now contribute only 5, which makes it advisable to now limit the maximum number of points to fit per galaxy to 5 to avoid overweighting some galaxies too much. On the other hand, for $r_F = 1.4$ kpc we have obtained $m \simeq 1.5 \times 10^{-22} \text{ eV c}^{-2}$ and $a_s \simeq 3.3 \times 10^{-77} \text{ m}$, a result which, although in our view obtained with an unnecessarily large value of r_F , is still in reasonably good agreement with the previous results.

This paper has been typeset from a $\text{\TeX}/\text{\LaTeX}$ file prepared by the author.

Table A1. Best-fit parameters (m , a_s , $\{M\}$). Also shown are the radii r_c and masses M_c of the halo cores and the enclosed masses within $r = 300$ pc (M_{300}) and corresponding mean densities ρ_{300} .

Galaxy	$m = 2.2 \times 10^{-22} \text{ eV c}^{-2}$		$a_s = 7.8 \times 10^{-77} \text{ m}$		
	M ($10^9 M_\odot$)	r_c (pc)	M_c ($10^8 M_\odot$)	M_{300} ($10^7 M_\odot$)	ρ_{300} ($10^{-1} M_\odot \text{ pc}^{-3}$)
UGCA444	0.24	997	1.03	0.47	0.41
NGC0024	1.89	861	8.09	5.60	4.95
UGC01281	0.19	1045	0.80	0.32	0.28
UGC05721	1.31	869	5.62	3.79	3.35
NGC3741	0.31	962	1.30	0.66	0.58
NGC3109	0.17	1066	0.73	0.27	0.24
NGC6789	1.78	862	7.62	5.26	4.65
UGC07603	0.51	913	2.16	1.27	1.12
KK98–251	0.12	1189	0.49	0.13	0.12
UGC07524	0.31	959	1.34	0.68	0.60
UGC07866	0.24	997	1.02	0.46	0.41
ESO444–G084	0.69	894	2.95	1.84	1.63
UGC05764	0.65	897	2.76	1.70	1.50
F5632	0.52	911	2.23	1.31	1.16
F5834	0.33	952	1.42	0.74	0.65
DDO154	0.19	1046	0.80	0.31	0.28
UGC07232	0.72	892	3.07	1.92	1.70